Fracture modeling of rocks based on random field generation and simulation of inhomogeneous domains

Clarke, P.L, Abedi, R.
Department of Mechanical, Aerospace & Biomedical Engineering, The University of Tennessee Space Institute, TN, USA

ABSTRACT: Realistic fracture simulations in rock as a heterogeneous brittle material with significant inherent randomness, require the use of models that incorporate its inhomogeneities and statistical variability. Since brittle materials do not match ductile materials in dissipating energy in the bulk, their fracture response is highly dependent on the stochastic microscale distribution and strength of defects. The high dependence of their fracture progress on microstructural defects results in wide scatter in their ultimate strength and the so-called size effect. Our approach for incorporating randomness in rocks is based on the modeling of stochastic volume elements (SVEs). Although representative volume elements (RVEs) are more commonly used in solid mechanics, SVEs are more appropriate for fracture analysis since they ensure that the material randomness is maintained. They still average microscale features similar to RVEs, and provide a more economical solution approach than those methods that explicitly model all microcracks in rock. To create a random field for macroscopic fracture strength field, we first generate several realizations of rock with a prescribed crack density and distribution. SVEs are then constructed with their centers at known spatial position on these random realizations. Next, by using a moving window approach, where the SVE traverses the known positions in these random realizations, we obtain first and second moments of the target random field. Point-wise probability distribution function and spatial covariance function are derived and used to generate consistent realizations of random fields based on the Karhunen-Loève (KL) method. Finally, such realizations will be used for the analysis of dynamic stimulation of a wellbore in a tight formation. A powerful and mesh adaptive spacetime discontinuous Galerkin finite element method is used for dynamic fracture simulations.

1 INTRODUCTION

Rocks, having highly random solid aggregates structure, are inhomogeneous at various scales. At microscale, heterogeneity is due to the presence of microcracks, granular microstructures which can include a large number of randomly oriented zones of potential failure in the form of grain boundaries. At macroscale, inherent homogeneity is the results of the matrix containing different rock types, and weak features such as faults and fracture networks. Rock inhomogeneities are crucial as they affect the continuum level mechanical characteristics such as strength, toughness, and elasticity properties of the material. These heterogeneities imposed by the rocks microstructure greatly influence the material peek and post-instability responses [1]. This is most evident in (quasi)brittle materials as they lack energy dissipative mechanisms to re-balance stresses induced by microscale stress concentrations. Another key aspect of brittle fracture, related to its dependence on material microstructure, is that for the same geometry and loading condition various crack patterns, ultimate loads, and absorbed energies

can be experienced [2–5]. These observations emphasize the importance of including randomness in material properties of rock in its fracture analysis.

Rock fracturing studies can *explicitly* or *implicitly* incorporate heterogeneities and/or discontinuous features within material models or computational approaches. Models derived from *explicit* approaches directly consolidate defects, microcracks, and other inhomogeneities into the scheme. Studies such as lattice models contain features making them favorable candidates to explicitly model material inhomogeneities. In that respect, a lattice of elements representative of a particle network are connected with springs [6] and heterogeneity is accounted for by varying strength and size of lattice particles [7]. However, the applications of explicit schemes are at times limited to small space and time scales because of the need to directly resolve existing microstructures.

An example of an implicit model is the probabilistic Weibull model. [8,9]. The Weibull model provides physical insight by accurately modeling size-effect (*i.e.,* the decrease of failure strength as a specimen size increases) in brittle materials. Continuum fracture models calibrated based on

a material's microstructure, such as the damage models of [10–13], are other examples of implicit approaches.

Furthermore, it is possible to derive macroscopic effective constitutive quantities with a homogenization approach wherein the elemental problem is solved in a *Volume Element* (VE). There are two commonly used classes of VEs known as *Representative Volume Element* (RVE) (which also is referred to as *Representative Elementary Volume* (REV) in rock mechanics), and its counterpart *Stochastic Volume Elements* (SVEs), *cf. e.g.,* [14–17]. A compilation of RVE definitions can be found in [18] but generally states that for an RVE to be valid it must: 1) be sufficiently smaller than the macroscale structure and sufficiently larger than microscale, 2) must contain a large number of micro-heterogeneities for the statistical homogeneous and ergodic properties to ensure proper representation of the macro response, and 3) have a response which is independent of the boundary condition type. When the size of a VE decreases, or the average microscopic feature size increases, the VE approaches the SVE regime which [19] deems as a more accurate averaging scheme than RVEs. The advantages of SVEs are that they can preserve material spatial heterogeneities and model stochastic fracture response from one sample to another one with exactly the same geometry and loading. The random fields that can be realized from SVEs by means of methods such as Karhunen-Loève (KL) expansion, used in works [20, 21], can be very effective and efficient for fracture analysis of brittle and quasi brittle materials as they preserve microstructure variability, but average it to a larger and more manageable length scale.

The authors have successfully used the Weibull model in the context of a spacetime discontinuous Galerkin finite element method [22] and demonstrated that having spatial inhomogeneity in fracture strength, through using a random crack nucleation model, can greatly improve predicted dynamic fracture patterns. In the present work, we want to derive the statistics of fracture strength field at the continuum macroscale based on the statistics of cracks in rock at microscale. Finally, a tight reservoir with a generated stochastic fracture random field is simulated in section 3.

2   FORMULATION

In this section the formulation is outlined for a scheme which allows the derivation of an analytical representation of correlated physics fields based on a material's microstructure, specifically for this work microcrack distribution in rocks. Section one presents a more formal definition of an SVE and how it is characterized. Section two presents the concept of the (non)Gaussian Karhunen-Loève expansion, the probability assumptions that accompany its derivation, and brief description on how it is solved numerically with finite element methods. Section three discusses the spatial sampling algorithm and spatial grid structure used to determine Cumulative Distribution Function (CDF) of a non-Gaussian random field and covariance of a Gaussian random field needed for implementation into the KL expansion. Section four introduces the equations

used to determine fracture strength which are extrapolated by employing the spatial sampling method. Finally, section five presents a dynamic stimulation of a wellbore where rock fracture strength is realized by the aforementioned stochastic approach.

2.1   Random Microstructure Characterization

Practically, it is not possible to fully determine the real microstructure of rock at every point in a large region such as a reservoir. These properties are supposed to be subsequently used for mechanical and fracture analysis. In lieu of using a deterministic approach where properties are provided at every point, the characterization of rock microstructure and obtaining of effective material properties are handled by statistical averaging in a continuum mechanics viewpoint, specifically by using Stochastic Volume Elements (SVE). To elaborate on the concept of SVEs, let us define the macroscale domain length L_M, microscale heterogeneity average length l_m and the SVE characteristic size L_{VE} seen in figure 1.

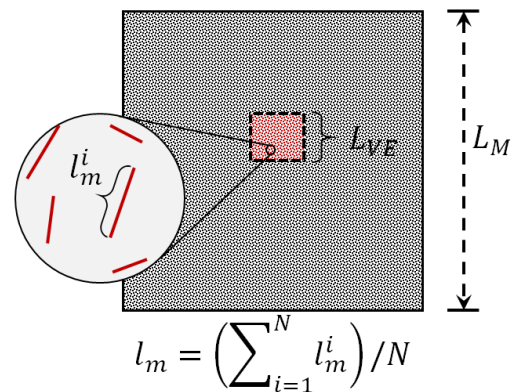$$l_m = \left(\sum_{i=1}^{N} l_m^i \right) / N$$

Figure 1: Macro- to Micro-scale length scales relevant to SVE homogenization.

The size of the SVE is affected by the characteristic length scale of the domain and the average length of microscale fractures. Assuming that the SVE is much smaller than the domain of interest ($L_{VE} \ll L_M$), the relative size of SVE to the contained microstructures is characterized through the ratio $\beta = L_{VE}/l_m$. As $\beta \to \infty$ the SVE approaches the RVE limit and randomness is lost given RVEs homogenize material properties and yield constant values from point to point for a macroscopically homogeneous material. A more detailed discussion on the relative sizes of an SVE to the domain and characteristic microstructure sizes is given in [19]; as discussed therein, in many cases of homogenization it is assumed that the RVE limit is reached (without verifying this condition in many cases). Roughly speaking and in practice, for RVEs β is often greater than 10 to 100, with higher values required when microstructural features are more complex, distinct from the bulk, or at higher densities. As discussed in the introduction, we specifically prefer to use SVEs to maintain spatial variability within one realization and sample to sample variations

across realizations. For SVEs, the size L_{VE} is chosen below the RVE limit to preserve randomness while observing the caveats that: 1) L_{VE} is larger than the microstructure length scale l_m and much smaller than the macroscopic length scale L_M, and 2) the SVE must contain a sufficient number of micro-heterogeneities to provide a comprehensive representation of the domain.

2.2 Karhunen-Loève (KL) Expansion

For a given domain $\bar{D}$ at an arbitrary location $\mathbf{x}$ a spatially-dependent correlated random field value $\eta(\mathbf{x})$ is to be determined. The value of this random field is derived based on a random variable ω which is of a probability structure known *a priori* (*i.e.*, $\eta = \eta(\mathbf{x}, \omega)$). In practice, it is not common to have an analytical representation of the random field or impossible to know its value at every discrete point within the domain but rather it is more likely that the values of the random field's expected value $\mathbb{E}(\eta(\mathbf{x})) = \mu_\eta(\mathbf{x})$ and covariance $COV_\eta(\mathbf{x}^1, \mathbf{x}^2)$ are known at a finite number of locations within the domain. Having these quantities (at all points), it is possible to derive a simple formula which approximates the mean and covariance of the known random variable distribution; a common method for producing such a formula is the Karhunen-Loève (KL) expansion of the random field $\eta = \eta(\mathbf{x}, \omega)$. The truncated KL expansion of the random field yields the following representation of the field,

$$\eta(\mathbf{x}, \omega) = \mu_\eta(\mathbf{x}) + \sum_{i=1}^{n_{KL}} \sqrt{\lambda_i} b_i(\mathbf{x}) Y_i(\omega)$$

where $\{\lambda_i, b_i(\mathbf{x})\}_{i=1}^{n_{KL}}$ are eigen-pairs determined from the covariance of the random field and $Y_i(\omega)$ are centered, uncorrelated random variables [1] which derive the probability distribution of the random field. Since the values of Y_is are independent if and only if they have spherical Gaussian (normal) distribution, in practice KL method is used for fields with point-wise Gaussian distribution. This, enables independent generation of random variables Y_i. Thus, we need to transfer a general random field to one with point-wise Gaussian distribution before using the KL method. This point is further elaborated when discussing (2) below. Thus, we assume that the KL expansion is carried out for a Gaussian random field $\eta(\mathbf{x}, \omega) \sim N(\mu_\eta, \sigma_\eta)$ (where σ_η is random field standard deviation),

$$\eta(\mathbf{x}, \omega) = \mu_\eta(\mathbf{x}) + \sum_{i=1}^{n_{KL}} \sqrt{\lambda_i} b_i(\mathbf{x}) y_i. \tag{1}$$

The aforementioned eigen-pairs are obtained by solving the generalized eigenvalue problem (EVP),

$$\int_{\bar{D}} COV_\eta(\mathbf{x}^1, \mathbf{x}^2) b(\mathbf{x}^2) d\mathbf{x}^2 = \lambda b(\mathbf{x}^1).$$

It is beneficial to note that due to the positive and symmetric nature of the covariance the eigenfunctions $b_i(\mathbf{x})$ are

real and orthogonal [2]. It is also important to note that all the eigenvalues λ_i are non-negative real values. The generalized eigenvalue problem is solved using a conventional Galerkin finite element method (CFEM) which allows the eigenfunction to be discretized over the spatial domain. The integral form of the EVP reduces to a generalized algebraic eigenvalue problem [23],

$$\mathbf{CD} = \mathbf{\Lambda BD}.$$

The N-dimension symmetric positive definite matrices $\mathbf{C}$, $\mathbf{B}$, and The N-dimension matrices $\mathbf{\Lambda}$ and $\mathbf{D}$ are defined as,

$$\mathbf{C}_{ij} = COV(\mathbf{x}^i, \mathbf{x}^j),$$
$$\mathbf{B}_{ij} = \int_{\bar{D}} h_i(\mathbf{x}) h_j(\mathbf{x}) d\mathbf{x},$$
$$\mathbf{\Lambda}_{ij} = \delta_{ij} \lambda_i,$$
$$\mathbf{D}_{ij} = d_i^{(j)},$$

where $\mathbf{x}^i$ and $\mathbf{x}^j$ are i-th and j-th finite element nodal degrees of freedom respectively for which covariance matrix term $\mathbf{C}_{ij}$ is evaluated. The above algebraic equation is solved for $\mathbf{\Lambda}$ and $\mathbf{D}$ (where the columns of $\mathbf{D}$ are the eigenvectors at each node of a prescribed FEM mesh) with $h_i(\mathbf{x})$ being the complete set of finite element shape functions.

In practice, the random field being approximated may in fact not be Gaussian; however, we can map a non-Gaussian $\xi(\mathbf{x}, \omega)$ to a Gaussian random field $\eta(\mathbf{x}, \omega)$ by using the CDF-inverse relation,

$$\eta(\mathbf{x}, \omega) = F_\eta^{-1}(F_\xi(\xi(\mathbf{x}, \omega))), \tag{2}$$

where F_ξ and F_η are the Cumulative Density Functions (CDF) of the non-Gaussian and Gaussian random fields, respectively. Subsequently, the KL method is used to generate random field realizations for the Gaussian field $\eta(\mathbf{x}, \omega)$ given that in (1) random variables y_i are independent, making their random generation practical. Finally, we can transfer the random field generated for the Gaussian field $\eta(\mathbf{x}, \omega)$ back to $\xi(\mathbf{x}, \omega)$ using the inverse of (2), *i.e.*, $\xi(\mathbf{x}, \omega) = F_\xi^{-1}(F_\eta(\eta(\mathbf{x}, \omega)))$.

2.3 Statistics of Random Microstructure: Spatial Sampling

Since the above KL expansion derivation requires the knowledge of covariance function $COV_\eta(\mathbf{x}^1, \mathbf{x}^2)$ and mean value of the random field $\eta(\mathbf{x}, \omega)$, we employ a spatial sampling method to extrapolate values for both field quantities utilizing stochastic volume elements (SVEs). Representative Volume Elements (RVEs) are frequently used to homogenized mechanical properties of materials; however, since for quasi-brittle materials spatial inhomogeneity, *i.e.*, microstructural variations, plays an important role in their fracture response, we employ SVEs to homogenize rock properties.

To statistically characterize a heterogeneous material we consider a finite set $D = \{\bar{D}_n; n \in [1, 2, ..., N]\}$

---

[1] $\mathbb{E}(Y_i(\omega)) = 0$, and $\mathbb{E}(Y_i(\omega) Y_j(\omega)) = 0$
[2] $\int_{\bar{D}} b_i(\mathbf{x}) b_j(\mathbf{x}) d\mathbf{x} = \delta_{ij}$

of N realizations $\bar{D}_n$. Each realization has a distribution of microscale fractures based on a prescribed probability structure and crack density. All realization domains are bounded by a boundary/surface Γ_D (*i.e.*, $\Gamma_D = \Gamma_{\bar{D}_1}, ..., \Gamma_{\bar{D}_N}$) and use the same (un)structured sampling grid of K points $\mathbf{x}^k = (x_1^k, ..., x_M^k); k \in [1, K]$. The sampling points define the center points of SVEs considered. This concept is shown in figure 2 for a 2 dimensional domain.
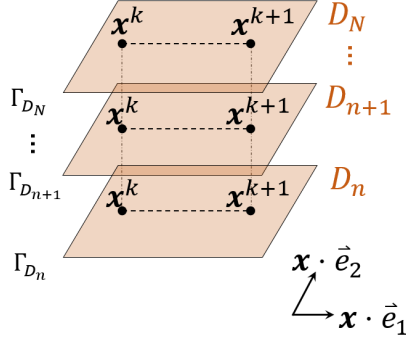

Figure 2: Spatial positions of sampled points inside each N realizations.

By forming SVEs centered at the grid points, a statistically averaged value of the material property considered is computed for each of these points based on its corresponding values across all N realizations. To have a better characterization of covariance function, we use a nonuniform sampling scheme where more SVEs are sampled close to the SVE in the center of the domain; that is, the incremental distance between two successive points is not uniform wherein it increases as the points are farther away from the domain center and closer to the boundary $\Gamma_{\bar{D}}$; this is seen in figure 3. This higher resolution about the domain center enables computing the covariance function more accurately, given that the values of the function tend to zero quickly as the distance of the two points increases.
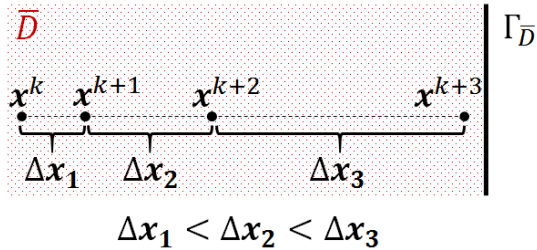

Figure 3: A nonuniform grid is used for better characterization of covariance function near zero.

By having the considered material property computed at all SVEs, *i.e.*, all sampled points across all SVEs, we can compute various statistical quantities for the given homogenized property, including its point-wise probability density function (PDF) and two-point covariance function. Let $\Theta(^n\mathbf{x}^k)$ be a property value extrapolated by an SVE within realization n at grid point k. The covariance

function between points $\mathbf{x}^p$ and $\mathbf{x}^q$ is computed as,

$$COV(\Theta(\mathbf{x}^p), \Theta(\mathbf{x}^q))$$
$$= \mathbb{E}(\Theta(\mathbf{x}^p)\Theta(\mathbf{x}^q)) - \mathbb{E}(\Theta(\mathbf{x}^p))\mathbb{E}(\Theta(\mathbf{x}^q))$$
$$= \sum_{n=1}^{N} \frac{(\Theta(\mathbf{x}_n^p) - \mathbb{E}(\Theta(\mathbf{x}^p)))(\Theta(\mathbf{x}_n^q) - \mathbb{E}(\Theta(\mathbf{x}^q)))}{N}, \quad (3)$$

where $p, q \in [1, ..., K]$. Considering that the values of the cumulative distribution function (CDF) $F(\Theta)$ and probability density function (PDF) $P(\Theta)$ are mutually dependent through the following relationship, it is sufficient to define only one of the two,

$$F(z) = \int_{-\infty}^{z} P(\chi)d\chi \quad (4a)$$

$$P(z) = \frac{\partial F(z)}{\partial z} \quad (4b)$$

Having a data set of $n_t = KN$ discrete values $\Theta(\mathbf{x}_n^p)$ ($1 \le p \le K, 1 \le n \le N$) with minimum Θ_{min}^s and maximum Θ_{max}^s values, the empirical cumulative distribution function is given as,

$$\forall \theta \;\; \Theta_{min}^s \le \theta \le \Theta_{max}^s : \quad \tilde{F}(\theta) = \frac{1}{n_t} \sum_{i=1}^{n_t} \mathbf{1}_{\chi_i \le \theta},$$

where $\mathbf{1}_A$ is the indicator of event A.

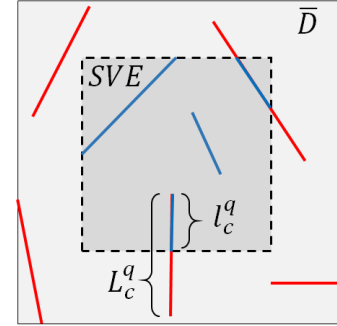## 2.4 Computation of fracture strength for an SVE

Figure 4: Cracks considered for computation of effective strength for an SVE: (blue line: considered crack segments internal to SVE, red line: neglected crack segments external to SVE)

In this section we describe how a fracture strength value is computed and assigned to an SVE. Figure 4 shows a sample SVE in domain $\bar{D}$. Beside the cracks that are inside the SVE, those that intersect its boundaries are also considered in deriving an effective strength for the SVE. The fracture strength is computed by finding the minimum unidirectional tensile stress, along all directions in $[0, \, 2\pi]$, such that at least for one of the crack tips in the SVE, $K = K_c$ where K is the stress intensity factor (SIF) at the crack tip and K_c is the fracture toughness of rock.

Underlying to this definition of fracture strength is that the propagation of microcracks is governed by linear elastic fracture mechanics (LEFM) theory and that upon the

propagation of the first microcrack the SVE basically can be considered as completely failed. The second assumption is justifiable as many results in the literature, see for example [24], demonstrate that for quasi-brittle RVEs and SVEs with microcracks and microdefects the load at which material response starts to deviate from linear elasticity is very close to the volume element's failure strength. This is due to the lack of considerable plastic deformation or other bulk energy dissipating mechanisms. In the context of our model for rock, wherein microcracks are randomly distributed, the point of major departure from linear elasticity is when the SIF for the most critical crack in the SVE reaches the fracture toughness. Finally, instead of doing a full FE analysis, we assume that the SIF of each crack can be approximated by that of a crack in an infinite domain. Clearly, this crude approximation ignores crack interactions, but is expected to provide relatively accurate representation for the macroscopic fracture strength field.

Let L_c and l_c be the original length and length of the qth microcrack within the SVE, respectively. The critical stress for this specific qth microcrack within the SVE is given by the equation

$$\bar{s}^{\,q} = \left(\frac{L_c^q}{l_c^q}\right)^{\alpha} \frac{K_c}{\sqrt{\pi L_c^q/2}},$$

where as mentioned K_c is the fracture toughness and α is a constant value coefficient. If $\alpha = 0$ we have $\bar{s}^{\,q} = K_c/\sqrt{\pi L_c^q/2}$ which is the critical tensile stress for a crack of length L^q in an infinite domain with fracture toughness K_c. On the other hand, if $\alpha = \frac{1}{2}$ we obtain $\bar{s}^{\,q} = K_c/\sqrt{\pi l_c^q/2}$, i.e., critical tensile stress for a crack of length l_c^q. Obviously, for cracks that are inside the domain, the value of α is irrelevant. However for those that intersect it, from the discussion above a value $\alpha = \frac{1}{2}$ only considers the part of the crack that is inside the SVE and $\alpha = 0$ models it as a full crack in the SVE. Given that the critical stress for such crack is clearly larger than the latter and should be considered lower than the former in deriving an effective critical stress for this crack in relation to the given SVE (considering that only a small fraction of the crack can be inside the SVE), we propose to use the intermediate value of $\alpha = \frac{1}{4}$. As discussed in section 4 with more physics-based approached we can obtain more realistic values for $\bar{s}^{\,q}$.
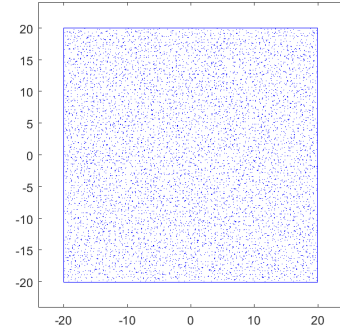
Once we compute critical stresses $\bar{s}^{\,q}$ for all cracks $q \in Q$ inside or intersecting a given SVE, the strength of the SVE $\bar{s}$ is defined as,
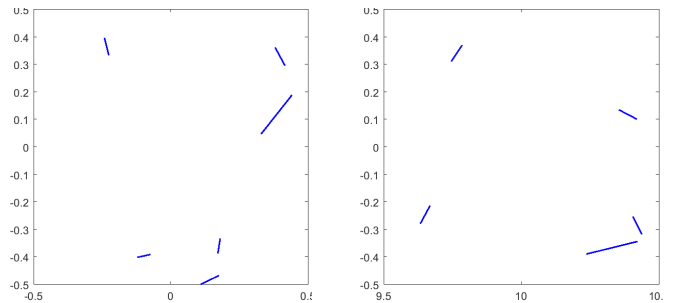
$$\bar{s} = min_{q \in Q}\{\bar{s}^{\,q}\}.$$

With this definition, a fracture strength is assigned to all SVEs, i.e., for all spatial positions and for all random realizations. These values are in turn used to compute PDF and covariance function from (4b) and (3), respectively. Finally, the KL method from section 2.2 is used to generate random fields whose statistics are consistent with the underlying microstructure (in this case rock with embedded microcracks).

2.5 Spacetime discontinuous Galerkin method

We use an *h*-adaptive spacetime discontinuous Galerkin (SDG) finite element method [25, 26] for our analyses of dynamic stimulation of a wellbore. This method uses basis functions which are discontinuous across all element boundaries. The SDG method directly discretizes spacetime using nonuniform grids that satisfy a special causality constraint [27]. This is contrary to conventional time marching schemes used for advancing the solution in time. These features yield unique properties such as local and asynchronous solution scheme, arbitrarily high and local temporal order of accuracy, and linear solution scaling with number of elements. Utilizing advanced adaptive operations in spacetime, and the local and asynchronous solution features of the SDG method, we can very accurately and efficiently capture complex fracture patterns by a *crack tracking* adaptive scheme [28, 29]. The solution is mesh independent and accommodates crack propagation in any desired direction, a feature similar to the popular XFEM and GFEM methods, but removes the need to enrich element basis functions. All these features make the SDG method ideal for dynamic rock fracture simulations reported in section 3.4.

(a) Example of realization $\bar{D}$ with random microstructure architecture.

(b) SVE sample from figure 5a centered at $\mathbf{x} = (0, 0)$.   (c) SVE sample from figure 5a centered at $\mathbf{x} = (120, 0)$.

Figure 5: A 40×40 domain and two sampled SVEs.

3 NUMERICAL RESULTS

The spatial domain $\bar{D}$ used for generating the following statistical data is a simple rectangular domain centered at the Cartesian position $\mathbf{x_{center}} = (0, 0)$ and spanning 40 length units in both $\vec{e}_1$ and $\vec{e}_2$ directions (*i.e.,*

$\mathbf{x} \in \bar{D} = [-20, 20] \times [-20, 20])$. An example of a realization containing the above spatial specifications is seen in figure 5a.

To generate rock domain realizations with microcracks, we need to assume a certain statistics for the microcracks; for the numerical results reported herein, we assume that the microcrack length follow a Weibull distribution [8, 9] and its angle is uniformly distributed between [0 2π] (that is there is no angular bias, as for example for rocks with bedding planes). Furthermore, the average and standard deviation of microcrack length are 20cm and 3.5cm, respectively. Finally, we use a take-and-place algorithm to distribute generated cracks in a domain of edge size $L_{\bar{D}} = 40$m. A sample realization is shown in figure 5a. It can clearly be seen that the average length lengths are smaller than the SVE size and the SVE size is much smaller than the domain size, conditions that were discussed in section 2.3. As discussed in section 2.3, the center points of sampled SVEs form a nonuniform grid. Two sample SVEs generated from the domain in figure 5a are shown in figures 5b and 5c.

3.1 The effect of the SVE size on random field statistics

The size of the SVE directly influences the statistics of the random field characterized. To study the relation between the SVE size and the fracture strength random field statistics, square SVEs with edge sizes of 1, 2, and 4 were considered. The PDFs of the fracture strength field in figure 6 are accordingly labeled by SVE**1 × 1**, SVE**2 × 2**, and SVE**4 × 4**.
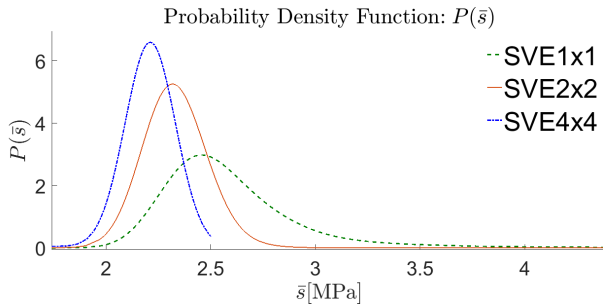

Figure 6: The effect of the SVE size on random field statistics.

As the SVE size becomes larger and tends to the RVE size limit, the peek of the PDF curve shifts to the left, that is a weaker material is represented. This is the well-known size effect for (quasi-)brittle materials; as the size of the domain increases there is a larger likelihood that a more critical crack or defect exists in it. That is why larger samples tend to have lower fracture strength. In fact, domain size calibrated Weibull model and many other stochastic models in the literature attempt to represent this phenomenon.

Another observation is that as the window size decreases, the sampled fracture strength values are more likely to have wider variations. The reason is that at small sizes, the SVE may land in a region with long crack(s) or a short one, thus yielding a low or a high fracture strength, respectively. This is demonstrated by higher standard deviations for smaller SVE window sizes in figure 6. On the contrary, as the SVE window size tends to the RVE limit size, the PDF tends to a Dirac delta function centered at the constant statistically averaged value. In this case, no matter where the volume element is sampled and which realization is considered, the crack ensemble represents macroscopically homogeneous value.[3] Clearly, the sizes considered herein are intentionally small (*i.e.,* the volume elements are SVEs) to capture rock strength variability. The following numerical results assume spatial sampling with an SVE length of one (*i.e.,* SVE1 × 1) as this size offered greater variability in fracture strength values but is large enough to not violate the requirements of the SVE containing a sufficient number of heterogeneities.

3.2 KL random fields

The KL random field meshes were generated based on two assumptions,

1. The material modeled was isotropic with a rotationally invariant scalar fracture strength, and the covariance function depending only on distance between two arbitrary points.

2. The sampled fracture strength values have log-normal probability distribution and covariance is calculated for strength values transformed to a standard normal distribution.

Assumption two means that instead of using CDF inverse approach, we used a log normal best fit for the PDFs in figure 6. Given the good level of fit we observed, this assumption is well-justified. Moreover, the covariance function for fracture strength, cast in the standard normal form (*cf.* section 2.2), is interpolated by the exponentially decaying function,

$$COV(\bar{s}(\mathbf{x}^1), \bar{s}(\mathbf{x}^2)) = e^{-\left(\frac{|\mathbf{x}^1 - \mathbf{x}^2|}{d_c}\right)^2},$$

where d_c is a characteristic correlation length scale implied by the form of the function.[4] Again, there was no hindrance in using the actual point-wise covariance function obtained by (3). However, the very good fit between the function form above, with $d_c \approx 0.386$, and the actual discrete covariance function was the rationale in using the analytical form for the function, which is shown in figure 7.

---

[3]For the RVE limit and the independence of fracture strength from the volume element center point, we are assuming a limiting strength exists as the volume element size tends to infinity and that rock is macroscopically homogeneous for fracture strength. Obviously, these assumptions can be relaxed and are not related to the SVE homogenization approach presented in this manuscript.

[4]Covariance function takes the value of one at zero relative distance, *i.e.,* $COV(\bar{s}(\mathbf{x}^1), \bar{s}(\mathbf{x}^1)) = 0$, because fracture strength field is first mapped to a standard normal distribution which has a point-wise covariance value of unity.
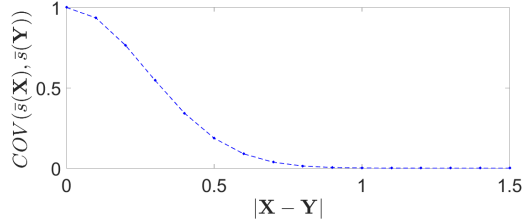
Figure 7: One-dimensional covariance function based on SVE1 × 1 results.

Solving the algebraic generalized eigenvalue problem with a Galerkin finite element method, the values for eigenvalues λ_n and eigenfunctions $b_n(\mathbf{x})$ were determined. The continuous and smoothly decreasing eigenvalues can be seen in figure 8.
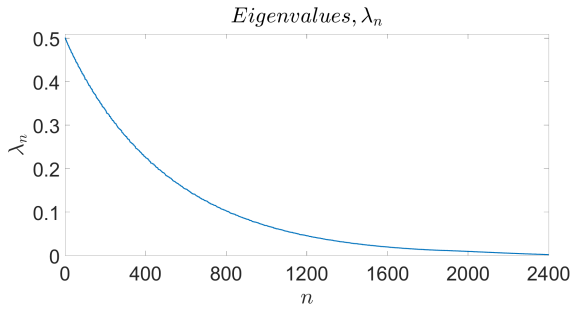

Figure 8: Eigenvalues λ_n for $COV(\bar{s}(\mathbf{x}^1), \bar{s}(\mathbf{x}^2)) \approx e^{-((|\mathbf{x}^1 - \mathbf{x}^2|)/0.386)^2}$, corresponding to SVE1 × 1 results.

For brevity only the corresponding eigenfunctions for $n = 1, 2, 4$, and 21 are shown in figure 9.

(a) Eigenfunction $b_1(\mathbf{x})$

(b) Eigenfunction $b_2(\mathbf{x})$

(c) Eigenfunction $b_4(\mathbf{x})$

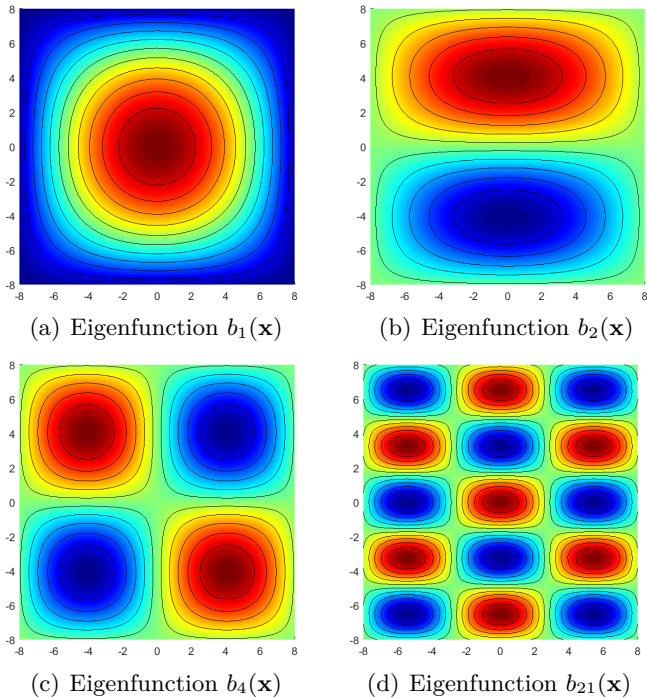(d) Eigenfunction $b_{21}(\mathbf{x})$

Figure 9: Eigenfunctions for $n = 1, 2, 4$, and 21 corresponding to eigenvalues in figure 8.

3.3 Discrete grids for fracture strength and FEM solution

A key feature of the random field discretization, using the Karhunen-Loève (KL) expansion method, is that the discrete mesh for fracture strength can be realized independent of the solid mechanics finite element mesh. Accordingly, finite element method discretization and mesh adaptive operations, *e.g.,* refinement and coarsening in spacetime [26, 29], can be performed without having to re-evaluate random fields which otherwise could lead to inaccurate and inconsistent random field values. For fracture simulations in section 3.4 a 16m × 16m domain is considered. Accordingly, a structured 2D mesh of dimensions $[-8, 8] \times [-8, 8]$ is used for KL expansion method. For this grid, 2D quadrilateral elements (100 × 100 elements) of equal element size are used for solving the eigenvalue problem and generating random field realizations. The KL discrete mesh is shown in figure 10.
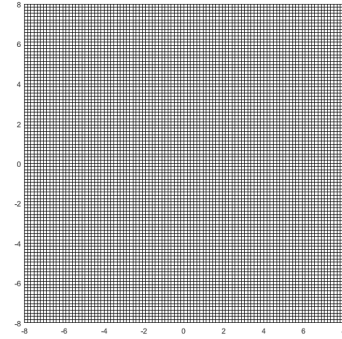

Figure 10: Structured spatial mesh for discretization of KL eigenvalue problem and random field realizations.

As mentioned in section 2.3 it is possible to transform a Gaussian random field $\eta(\mathbf{x})$ to a non-Gaussian $\xi(\mathbf{x})$ knowing the cumulative distribution function of both reference and target field distribution. With the assumption that the original sampled fracture strength has a log normal distribution this transformation simplifies to the form,

$$\xi(\mathbf{x}) = e^{\mu_\eta + (\eta(\mathbf{x})\sigma_\eta)},$$

where μ_η and σ_η are the mean and standard deviation of the Gaussian random field which in this case can be determined from the known mean μ_ξ and standard deviation σ_ξ of the log-normal field by the following equation,

$$\sigma_\eta = \sqrt{ln\left(1 + \frac{\sigma_\xi}{\mu_\xi^2}\right)}.$$

$$\mu_\eta = ln\left(\frac{\mu_\xi}{\sqrt{1 + \frac{\sigma_\xi}{\mu_\xi^2}}}\right).$$

The effective non-Gaussian random field $\xi_{eff}(\mathbf{x}) = \bar{s}(\mathbf{x})$ that is used in rock fracture simulations is $\bar{s}(\mathbf{x}) = \bar{s}_{min} + \xi(\mathbf{x})$ where $\bar{s}_{min}$ is the minimum value obtained during the SVE sampling algorithm. Figure 11a is a visualization of the random field realization number one for correlation length $d_c \approx 0.386$m. This random field for

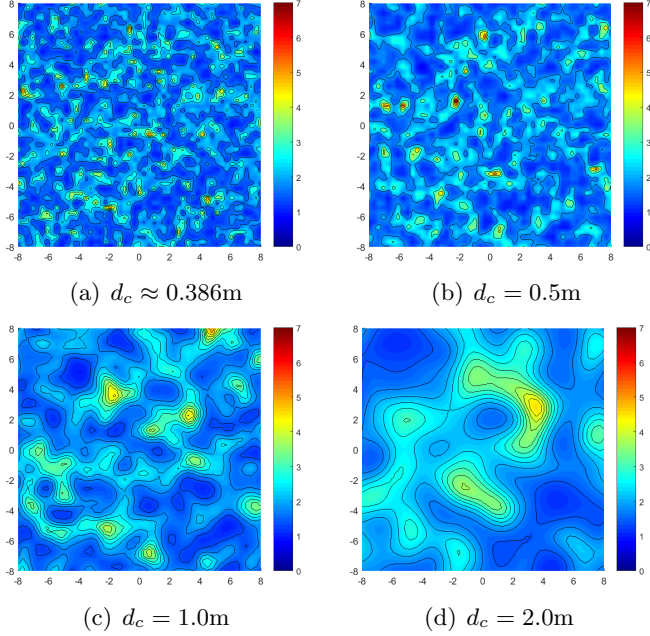fracture strength is used for the reference dynamic rock fracture simulation in section 3.4.

(a) $d_c \approx 0.386$m

(b) $d_c = 0.5$m

(c) $d_c = 1.0$m

(d) $d_c = 2.0$m

Figure 11: The first realization of KL-generated grids for fracture strength of different correlation lengths, $d_c \approx 0.386$m and $d_c = 0.5$m, 1.0m, 2.0m.

Before presenting dynamic fracture results, the effect of covariance function correlation length d_c on the KL random field solution is discussed. Figure 11 depicts random field solutions for correlation length scales $d_c \approx 0.386$m, and $d_c = 0.5$m, 1.0m, 2.0m. As the correlation lengths tend to zero there is a faster decline in the correlation of values between two points as the points become farther apart relative to the given correlation length scale d_c. The correlation decreases result in high variability of random field values within an arbitrarily small area. Smaller correlation lengths could potentially be obtained from sampling of a rock formation with higher variability in the location and strength of defects and using smaller SVE window sizes.

3.4 Dynamic stimulation of a wellbore with random fracture strength

Herein, we demonstrate the use of generated random fracture fields for the analyses of dynamic stimulation of a wellbore in a tight reservoir. We choose a hybrid propellant method where loading is applied at highly dynamic rates [30, 31], but similar to hydraulic fracturing the pressure is applied through perforations on the sides of the wellbore. Figure 12 shows the set-up of the problem where a circular wellbore, subjected to confinement pressure $\sigma_h = \sigma_H = 2.425$ MPa, is located in the center of a 16m × 16m rectangular domain. The wellbore is perforated at four distinct angular locations, *i.e.,* 0 rad, $\pi/2$ rad, π rad, and $3\pi/2$ rad, which upon loading promotes propagation in those directions. The dynamic pressure load, applied on the perforation surfaces, ramps up

from ambient pressure to a maximum value of 23.0MPa in 10 ms. The bulk material properties are: Young's Modulus $E = 20$ GPa, mass density $\rho = 2500$ kg/m^3, and Poisson's ratio $\nu = 0.20$.

The values of fracture strength $\bar{s}(\mathbf{x})$ are extracted from the independent KL random field solution discretization. The fracture strength equation parameters used in the SVE sampling algorithm are fracture toughness $K_c = 1.13\text{MPa}\sqrt{m}$ and coefficient $\alpha = \frac{1}{4}$. For 1×1 SVE sampling size, this resulted in mean value, standard deviation, and minimum value of fracture strength equal to $\mathbb{E}(\bar{s}) = 2.2$ MPa and $\sigma_{\bar{s}} = 455$ kPa, and $\bar{s}_{\min} = 1.34$ MPa, respectively.
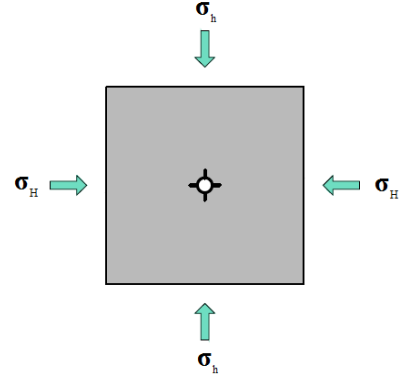

Figure 12: Problem sketch for dynamic stimulation of a wellbore.

Figure 13 shows a sequence of visualization of the problem with SVE1×1 fracture strength random field values. The first realization shown in fig 11a is used for this simulation. Figures 13a and 13b show stages right before and after the main cracks bifurcate, respectively. In figure 13c, cracks start to bifurcate and induce microcracking more frequently because the cracks are accelerating and the applied pressure load on crack surfaces is still ramping up. Finally, in figure 13d the existence of regions of high kinetic and strain energy densities, mapped to height and color fields respectively, corresponds to a highly transient crack propagation regime. Crack path oscillation, microcracking, and crack bifurcation are all mechanisms in which quasi-brittle materials such as rocks dissipate high input energy power.

By using the KL random field solutions seen in figures 11a, and a domain of homogeneous fracture strength we wanted to investigate the effect of incorporating variability in fracture strength field on fracture response. In figures 14 and 15 finite element space front and deformed shaped of fracture network are compared for solutions obtained with KL random field solution with correlation length $d_c \approx 0.386$m, and spatially homogeneous fracture strength $\bar{s} = 2.2$ MPa (which matched the mean value of the mesh generated by SVE1×1) at time $t = 4.2ms$.

Figure 14 is better suited to observe high levels of mesh refinement around moving crack tips, while the fracture patterns can more clearly be seen in figure 15. Herein, we use the interfacial damage model from [28] to represent processes of surface debonding on a fracture interface. In
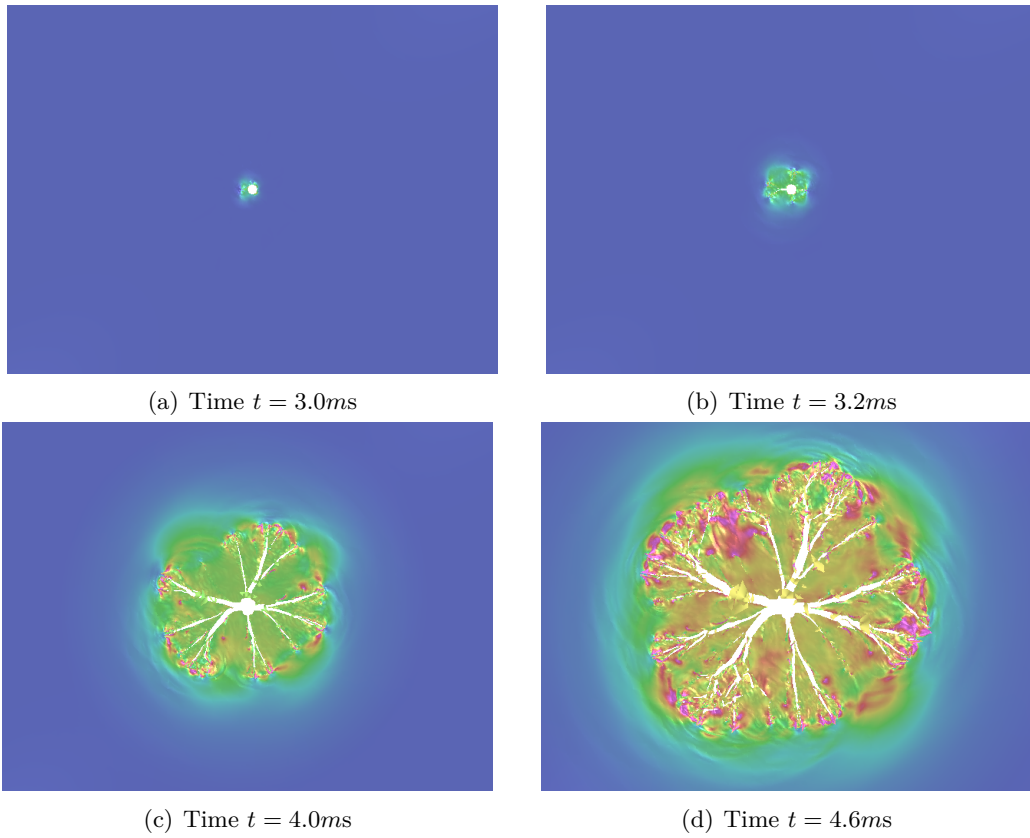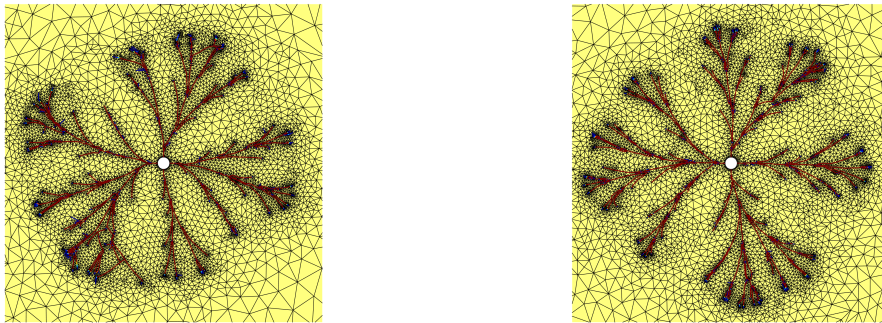
(a) Time $t = 3.0ms$

(b) Time $t = 3.2ms$

(c) Time $t = 4.0ms$

(d) Time $t = 4.6ms$

Figure 13: A series of solution visualization of dynamic wellbore stimulation. Fracture strength values are based on the KL mesh in figure 11a for SVE1 × 1. Strain energy and height fields are mapped to color and height fields respectively.

(a) Variable fracture strength for $d_c \approx 0.386$m.

(b) Constant fracture strength $\bar{s} = 2.2$ MPa.

Figure 14: Comparison of finite element space mesh for random and nonrandom fracture strength, at time $t = 4.2m$s.

(a) Variable fracture strength for $d_c \approx 0.386$m.

(b) Constant fracture strength $\bar{s} = 2.2$ MPa.

Figure 15: Comparison of deformed shape for random and nonrandom fracture strength, at time $t = 4.2m$s.

both figures, damage value is mapped to color with the range blue to red denoting zero to full interfacial damage. As we observe, in all cases except in fracture process zones right in the wake of crack tips, the rest of crack segments experience full damage. That is, as expected regions that are supposed to be physically debonded have a damage value of one.

Fracture patterns for random fracture strength are shown in figures 14(a) and 15(a). With the results for the homogeneous fracture strength, *cf.* figures 14(b) and 15(b), we observe some distinctions between these results and those obtained with KL random field solutions. Specifically, incorporating fracture strength randomness, in lieu of a homogeneous value, results in fracture patterns with slightly fewer microcracks and crack branching. Also, the fracture patterns obtained with variable fracture strength are less symmetric with respect to horizontal and vertical lines passing through the center of the wellbore. We attribute this to local variations in fracture strength that can further break the symmetries implied by the geometry and loading for this problem.

4   CONCLUSIONS

By using stochastic volume elements, and by assuming that at the microscale defects in the form of microcracks populate rock, we used a stochastic approach to generate random fields for fracture strength of rocks. A set of rock domain realizations were spatially sampled using nonuniform grids wherein an SVE was constructed at each grid point. By using an approximate equation, which ignored the interaction of individual cracks, we assigned a fracture strength value to each SVE. Thereafter, distribution statistics (*i.e.,* probability density, cumulative distribution, covariance) based on a non-Gaussian probability structure were determined. By solving an algebraic generalized eigenvalue problem with finite element method we determined eigenvalue and eigenfunction pairs used in the Karhunen-Loève expansion of a Gaussian random field. The KL random field was subsequently transformed to reflect the probability structure of the originally sampled non-Gaussian random field through a simple cumulative density function relationship. This obtained non-Gaussian random field randomizes fracture strength values for fracture analysis of rocks.

In this work we assumed a certain statistics for in-situ microcracks in rock. In future works we aim to use actual microcrack statistics such as those reported in [32] and employ more robust approaches for generation of microcracked domains as in [33, 34]. We also ignored the interaction of microcracks in the computation of stress intensity factors. For each SVE by solving a few simple boundary loading conditions using finite element methods, we can calculate stress intensity factors for each crack for any macroscopic direction of applied tension. This enables the derivation of more accurate, and angular–dependent fracture strengths at the SVE level. In turn, this would better demonstrate the differences in fracture response obtained by a stochastic model for fracture strength, con-

sistent with underlying microcrack distribution, and the models that assume a spatially uniform fracture strength. Although treating fracture strength as a random field appears to be more important than elastic moduli, we plan to determine their individual statistics as well as mutual cross-correlations. Since these quantities are not expected to be mutually independent, we also intend to generalize the presented work and simultaneously generate random fields for more than one scalar field.

REFERENCES

[1] Yin, X., W. Chen, A. To, C. McVeigh, and W.K. Liu (2008) Statistical volume element method for predicting microstructure-constitutive property relations. *Computer Methods in Applied Mechanics and Engineering*, **197**, 3516–3529.

[2] Al-Ostaz, A. and I. Jasiuk (1997) Crack initiation and propagation in materials with randomly distributed holes. *Engineering Fracture Mechanics*, **58**, 395–420.

[3] Carmeliet, J. and H. Hens (1994) Probabilistic nonlocal damage model for continua with random field properties. *Journal of Engineering Mechanics*, **120**, 2013–2027.

[4] Sobczyk, K. (2008) Morphological complexity of material microstructures: From stochastic models to fracture estimation. *Probabilistic Engineering Mechanics*, **23**, 444–455.

[5] Daphalapurkar, N.P., K.T. Ramesh, L. Graham-Brady, and J.F. Molinari (2011) Predicting variability in the dynamic failure strength of brittle materials considering pre-existing flaws. *Journal of the Mechanics and Physics of Solids*, **59**, 297–319.

[6] Schlangen, E. and E.J. Garboczi (1997) Fracture simulations of concrete using lattice models: Computational aspects. *Engineering Fracture Mechanics*, **57**, 319–332.

[7] Li, Jia (2000) Debonding of the interface as 'crack arrestor'. *International Journal of Fracture*, **105**, 57–79.

[8] Weibull, W. (1939) A statistical theory of the strength of materials. *R. Swed. Inst. Eng. Res.*, p. Res. 151.

[9] Weibull, W. (1951) A statistical distribution function of wide applicability. *Journal of Applied Mechanics*, **18**, 293–297.

[10] Taylor, Lee M., Er-Ping Chen, and Joel S. Kuszmaul (1986) Microcrack-induced damage accumulation in brittle rock under dynamic loading. *Computer Methods in Applied Mechanics and Engineering*, **55**, 301 – 320.

[11] Homand-Etienne, F., D. Hoxha, and J.F. Shao (1998) A continuum damage constitutive law for brittle rocks. *Computers and Geotechnics*, **22**, 135–151.

[12] Shao, J.F. and J.W. Rudnicki (2000) A microcrack-based continuous damage model for brittle geomaterials. *Mechanics of Materials*, **32**, 607 – 619.

[13] Lu, Y.L., D. Elsworth, and L.G. Wang (2013) Microcrack-based coupled damage and flow modeling of fracturing evolution in permeable brittle rocks. *Computers and Geotechnics*, **49**, 226–44.

[14] Baxter, S.C. and L.L. Graham (2000) Characterization of random composites using moving-window technique. *Journal of Engineering Mechanics*, **126**, 389–397.

[15] Tregger, N., D. Corr, L. Graham-Brady, and S. Shah (2006) Modeling the effect of mesoscale randomness on concrete fracture. *Probabilistic Engineering Mechanics*, **21**, 217–225.

[16] Segurado, J. and J. LLorca (2006) Computational micromechanics of composites: The effect of particle spatial distribution. *Mechanics of Materials*, **38**, 873–883.

[17] Koyama, Tomofumi and Lanru Jing (2007) Effects of model scale and particle size on micro-mechanical properties and failure processes of rocks—a particle mechanics approach. *Engineering Analysis with Boundary Elements*, **31**, 458 – 472, innovative Numerical Methods for Micro and Nano Mechanics and Structures - Part I Innovative Numerical Methods for Micro and Nano Mechanics and Structures - Part I.

[18] Pelissou, C., J. Baccou, Y. Monerie, and F. Perales (2009) Determination of the size of the representative volume element for random quasi-brittle composites. *International Journal of Solids and Structures*, **46**, 2842 – 2855.

[19] Du, X. and M. Ostoja-Starzewski (2006) On the scaling from statistical to representative volume element in thermoelasticity of random materials. *Networks and Heterogenous Media*, **1**, 259 – 274.

[20] Xu, X.F. and L. Graham-Brady (2005) A stochastic computational method for evaluation of global and local behavior of random elastic media. *Computer Methods in Applied Mechanics and Engineering*, **194**, 4362 – 4385.

[21] Shang, Shen and Gun Jin Yun (2013) Stochastic finite element with material uncertainties: Implementation in a general purpose simulation program. *Finite Elements in Analysis and Design*, **64**, 65 – 78.

[22] Abedi, R., O. Omidi, and P.L. Clarke (2016) Numerical simulation of rock dynamic fracturing and failure including microscale material randomness. *Proceeding: 50th US Rock Mechanics/Geomechanics Symposium, June 26-June 29, Houston, Texas - USA*, pp. ARMA 16–0531 (13 pages).

[23] Ghanem, R. and P.D. Spanos (1991) *Stochastic finite elements: a spectral approach*. Springer-Verlag.

[24] Nguyen, Vinh Phu, Oriol Lloberas-Valls, Martijn Stroeven, and Lambertus Johannes Sluys (2011) Homogenization-based multiscale crack modelling: From micro-diffusive damage to macro-cracks. *Computer Methods in Applied Mechanics and Engineering*, **200**, 1220–36.

[25] Abedi, Reza, Robert B. Haber, and Boris Petracovici (2006) A spacetime discontinuous Galerkin method for elastodynamics with element-level balance of linear momentum. *Computer Methods in Applied Mechanics and Engineering*, **195**, 3247–3273.

[26] Abedi, R., R. B. Haber, S. Thite, and J. Erickson (2006) An *h*–adaptive spacetime–discontinuous Galerkin method for linearized elastodynamics. *Revue Européenne de Mécanique Numérique (European Journal of Computational Mechanics)*, **15**, 619–642.

[27] Abedi, Reza, Shuo-Heng Chung, Jeff Erickson, Yong Fan, Michael Garland, Damrong Guoy, Robert Haber, John M. Sullivan, Shripad Thite, and Yuan Zhou (2004) Spacetime meshing with adaptive refinement and coarsening. *Proceedings of the Twentieth Annual Symposium on Computational Geometry*, June 9-11, pp. 300–309, SCG '04, ACM.

[28] Abedi, Reza (2010) *Spacetime damage-based cohesive model for elastodynamic fracture with dynamic contact*. Ph.D. thesis, Department of Theoretical and Applied Mechanics, University of Illinois at Urbana–Champaign.

[29] Omidi, Omid, Reza Abedi, and Saeid Enayatpour (2015) An adaptive meshing approach to capture hydraulic fracturing. *The 49th US Rock Mechanics/Geomechanics Symposium, June 28-July 1, San Francisco,CA,USA*.

[30] Hanson, JM, RA Schmidt, CH Cooley, JF Schatz, et al. (1984) Multiple fracture stimulation using controlled pulse pressurization. *SPE Unconventional Gas Recovery Symposium*, Society of Petroleum Engineers.

[31] Omidi, Omid, Reza Abedi, and Saeid Enayatpour (2016) Well stimulation in tight formations: a dynamic approach. *Proceeding: 50th US Rock Mechanics/Geomechanics Symposium, June 26-June 29, Houston, Texas - USA*, pp. ARMA 16–0150 (12 pages).

[32] Olarewaju, Joseph, Saleem Ghori, Alhasan Fuseni, Mohammed Wajid, et al. (1997) Stochastic simulation of fracture density for permeability field estimation. *Middle East Oil Show and Conference*, Society of Petroleum Engineers.

[33] Graham-Brady, Lori (2010) Statistical characterization of meso-scale uniaxial compressive strength in brittle materials with randomly occurring flaws. *International Journal of Solids and Structures*, **47**, 2398–2413.

[34] Huq, F., R. Brannon, and L. Graham-Brady (2016) An efficient binning scheme with application to statistical crack mechanics. *International Journal for Numerical Methods in Engineering*, **105**, 33–62.